ACS Catalysis

Research Article

pubs.acs.org/acscatalysis

Metal Chalcogenide Nanofilms: Platforms for Mechanistic Studies of Electrocatalysis

Joseph M. Falkowski and Yogesh Surendranath*

Department of Chemistry, Massachusetts Institute of Technology, 77 Massachusetts Avenue, Cambridge Massachusetts 02139, United States

Supporting Information

ABSTRACT: The systematic development of improved electrocatalysts requires strategies for preparing candidate materials as well-defined thin-film electrodes that are amenable to straightforward characterization of reaction mechanism and catalyst specific activity. While numerous thin film preparation methods are established for transition metals and metal alloys, few strategies exist for transition metal chalcogenides, despite growing recognition of their role as potent electrocatalysts. Herein we show that electrochemical atomic layer deposition (E-ALD) is a powerful tool for accessing well-defined metal chalcogenide electrocatalysts, by synthesizing, for the first time, crystalline conformal films of Co_9S_8, a promising earth-abundant oxygen reduction catalyst, with tunable nanoscale thickness. The as-prepared nanofilms display relatively high activity for the oxygen reduction reaction and provide a robust platform for detailed mechanistic investigations. Initial mechanistic studies reveal that oxygen reduction on Co_9S_8 nanofilms proceeds via rate-limiting one-electron transfer to O_2 with a specific activity of 20.6 μA cm^{-2} at 600 mV vs RHE. This study opens the door to the systematic application of E-ALD to investigate chalcogenide electrocatalysts across the transition series.

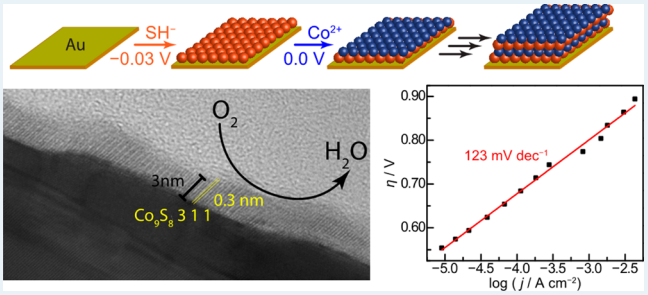

KEYWORDS: *E-ALD, metal chalcogenide, electrocatalysis, mechanistic studies, oxygen reduction, thin films*

The interconversion of electrical and chemical energy can be achieved at the polarized interfaces of spatially separated electrodes found commonly in batteries, electrolyzers, and fuel cells. For complex multielectron energy conversion reactions such as oxygen reduction,[1,2] hydrogen evolution,[3,4] and water oxidation,[5,6] these electrodes must be decorated with catalysts that increase the reaction efficiency and/or selectivity. Thus, the electrochemical evaluation of any heterogeneous catalyst candidate invariably requires its fabrication as a thin film on an inert electrode substrate. Commonly, nanoparticulate electrocatalysts are fashioned into electrodes by combining them with a conductive carbon and binder to generate a disordered, mesoporous catalyst-impregnated network. While this method generates high geometric current densities, these electrodes are ill-suited to detailed mechanistic studies because of inhomogeneous electron and ion transport limitations[7,8] and potential secondary reactions within the mesoporous network.[9] Moreover, except in the case of precious metals, which exhibit surface adsorption features that can be used to measure electroactive surface area,[10,11] it is difficult to isolate catalyst specific activity, impeding straightforward comparisons between different catalyst candidates. These challenges can be overcome if catalysts can be accessed as smooth thin films on inert electrodes such that transport to the surface is uniform and the electroactive area reflects that of the underlying substrate.

For transition metal and metal alloy catalysts, the preparation of relatively smooth electrode surfaces can be achieved readily by evaporation onto an inert substrate[12,13] or polishing of a single or polycrystalline bulk solid.[14] These tools have been instrumental in advancing our mechanistic understanding of important energy conversion reactions on metal and metal alloy surfaces. However, analogous strategies for accessing uniform thin films of transition metal chalcogenides are limited, despite recent recognition of their role as potent electrocatalysts for a wide range of energy conversion reactions including oxygen evolution,[15] oxygen reduction,[16] hydrogen evolution,[17−19] and CO_2 reduction.[20,21]

Here, we show that electrochemical atomic layer deposition (E-ALD) is a powerful strategy for accessing model metal chalcogenide electrocatalysts. E-ALD, which involves sequential self-limiting electrodeposition of metal and chalcogenide ions, has been applied extensively to synthesize II−VI and IV−VI semiconductor thin films on electrode substrates,[22] but has yet to be applied to the preparation of transition metal chalcogenide electrocatalysts. As a potent example, we report a novel room temperature E-ALD preparation of crystalline conformal Co_9S_8 films of tunable nanometer thickness (nanofilms). Co_9S_8 is a promising catalyst for the oxygen

Received: March 3, 2015
Revised: April 20, 2015
Published: April 21, 2015

ACS Publications © 2015 American Chemical Society

DOI: 10.1021/acscatal.5b00449
ACS Catal. 2015, 5, 3411−3416

reduction reaction (ORR), the efficiency-limiting reaction in nearly all low-temperature fuel cells,[1,23] because of its extremely low cost, high tolerance to impurities in the fuel stream, and wide pH range of operation.[18,24] Indeed, ab initio simulations suggest that Co_9S_8 can display activities rivaling platinum.[25] However, there is a paucity of mechanistic insight on ORR mediated by cobalt sulfide because studies up until this point have employed nanoparticles dispersed onto high surface area carbon supports,[26] which do not lend themselves to rigorous mechanistic investigation. Indeed, the specific activity of this material has never been reported because of the inability to estimate the electroactive surface area of a disordered carbon−nanoparticle composite film. The Co_9S_8 nanofilms reported here uniformly coat the underlying gold substrate and are catalytically active for the ORR as prepared, providing, for the first time, direct mechanistic insight into the rate-limiting step and specific activity for the ORR on this promising material.

To build up a uniform cobalt sulfide layer of arbitrary thickness, we utilize a series of surface self-limiting electrochemical reactions that permit sequential deposition of Co and S onto a gold substrate (Figure 1). Electrodeposition of a sulfur

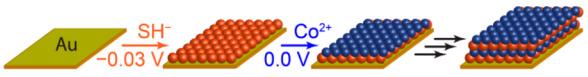

Figure 1. Layer-by-layer electrosynthesis of thin film cobalt sulfide ORR catalysts on Au electrodes.

adlayer on polycrystalline gold electrodes initiates the layer-by-layer growth. Exposure of a gold electrode held at the open circuit potential to 0.25 M $(NH_4)_2SO_4$, pH 9.6 electrolyte containing 2.2 mM NaSH leads to spontaneous adsorption of sulfur,[19] and the surface coverage of this adlayer can be tuned through partial reductive desorption as revealed by linear sweep voltammograms (LSVs) (Figure 2). A broad cathodic wave corresponding to partial stripping of this sulfur layer[19b] is observed at $E_{p,c}$ = 0.03 V (all potentials are reported versus the reversible hydrogen electrode, RHE). Controlled potential electrolysis at −0.03 V, 60 mV beyond the peak of this wave, was found to be optimal for preparation of cobalt sulfide thin films.

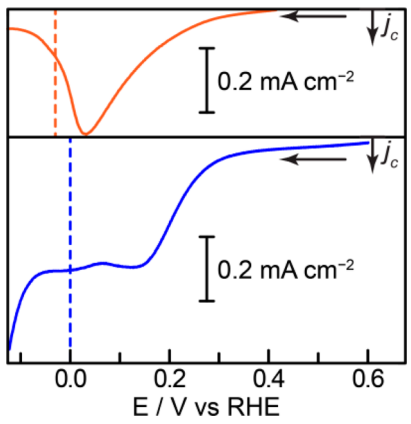

Figure 2. LSVs (50 mV s^{-1} scan rate) of a native Au electrode in 0.25 M $(NH_4)_2SO_4$, pH 9.7 electrolyte containing 2.2 mM NaSH (top) and a sulfidized Au electrode in 10 mM $Na_2B_4O_7$, 0.1 M $NaClO_4$, pH 6.7, electrolyte containing 5 mM $CoSO_4$ (bottom). Red and blue dotted vertical lines indicate potentials chosen for sulfur and cobalt deposition, respectively.

An LSV of this sulfur-modified Au electrode recorded in 10 mM sodium borate, 0.1 M $NaClO_4$ electrolyte, pH 6.7, containing 5 mM $CoSO_4$ reveals a broad cathodic feature at $E_{p,c}$ = 0.12 V. This feature is absent on a native Au electrode (Figure S1) and on a sulfur-modified Au electrode in Co^{2+}-free electrolyte (Figure S2). Additionally, the peak current scales linearly with scan rate (Figures S3 and S4), and the peak potential is 0.20 V positive of the bulk cobalt deposition wave, which onsets at −0.08 V (Figure 2, bottom). Chronoamperometry at 0.0 V gives rise to a self-limiting adlayer of Co as determined by the saturation in oxidative desorption charge, independent of the time duration of reductive electrodeposition (Figures S5 and S6). Together, these observations indicate that this wave at 0.12 V is due to underpotential deposition of a self-limiting adlayer of Co templated by the sulfur adlayer.

Similar cathodic features for Co and S are observed in subsequent LSV scans after the formation of the first S and Co adlayers (Figure S7). Exploiting this behavior, we prepared thin films of tunable thickness via sequential controlled potential electrolysis at −0.03 V (Figure 2, dotted red line) and 0.0 V (Figure 2, dotted blue line) in the S and Co deposition solutions, respectively. To facilitate rapid and reproducible film preparation, sequential self-limiting electrolysis was conducted in a low-volume flow cell in line with computer-controlled peristaltic pumps for rapid solution exchange (see the SI for detailed synthetic protocols).

To further investigate the structure of these thin films, we examined their atomic composition by ex situ inductively coupled plasma mass spectrometry (ICP-MS) of nitric acid-digested samples. Increasing numbers of deposition cycles gave rise to a linear increase in the quantity of Co on the surface (Figure S8), evincing the highly tunable nature of this deposition method. X-ray photoelectron spectroscopy (XPS) (Figures S9−S11) reveals a cobalt-to-sulfur ratio of approximately 1:1, consistent, within the measurement error, with the Co:S ratios found in the pentlandite (C_9S_8) phase of cobalt sulfide. Additionally, XPS spectra of catalyst films reveal two peaks at 778 and 781 eV (Figure S10). The higher binding energy feature disappears following brief (500 nA for 6 s at 1000 V) argon sputtering and ORR catalysis (see below), suggesting that it may result from adventitious surface oxides. Notwithstanding, the observed XPS peaks are in line with Co $2p^{3/2}$ peaks observed in bulk preparations of Co_9S_8.[23e] Together, the data corroborate that layer-by-layer electrodeposition provides access to cobalt sulfide films of tunable thickness.

To gain insight into the nanoscale morphology of our electrodeposited layer, we used a combination of cross-sectional transmission electron microscopy (TEM) and atomic force microscopy (AFM). A polycrystalline gold electrode modified with ten deposition cycles of cobalt sulfide was subjected to fast ion bombardment milling (see the SI for details of sample preparation) to produce a thin (∼80 nm) cross-section of the Au|CoS_x interface. Representative TEM images of this cross section are shown in Figure 3 and Figure S12 and reveal a high-contrast region corresponding to bulk gold terminated by a low-contrast region corresponding to the conformal cobalt sulfide film. The amorphous carbon film deposited during microfabrication of the cross-sectional slice is observed on the opposite side of the cobalt sulfide layer. Remarkably, the electrodeposited layer displays clear lattice fringing indicative of crystalline domains on the surface of the gold substrate. Fourier transform of the TEM image of the cobalt sulfide layer reveals

DOI: 10.1021/acscatal.5b00449
ACS Catal. 2015, 5, 3411−3416

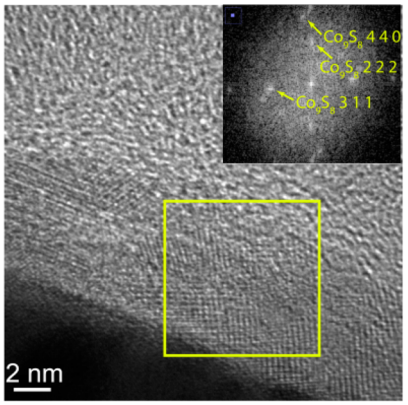

Figure 3. Cross-sectional TEM image of a cobalt sulfide film prepared from 10 deposition cycles on a polycrystalline Au electrode. Fast Fourier transform (FFT) of the cobalt sulfide layer with indices corresponding to Co_9S_8 (inset).

lattice spacings corresponding to the 311, 222, and 440 planes of the pentlandite phase, Co_9S_8. Consistent with this phase assignment, grazing incidence X-ray diffraction shows the principle of only the principle Co_9S_8(311) and Au(111) peaks with no other diffraction observable (Figure 4).

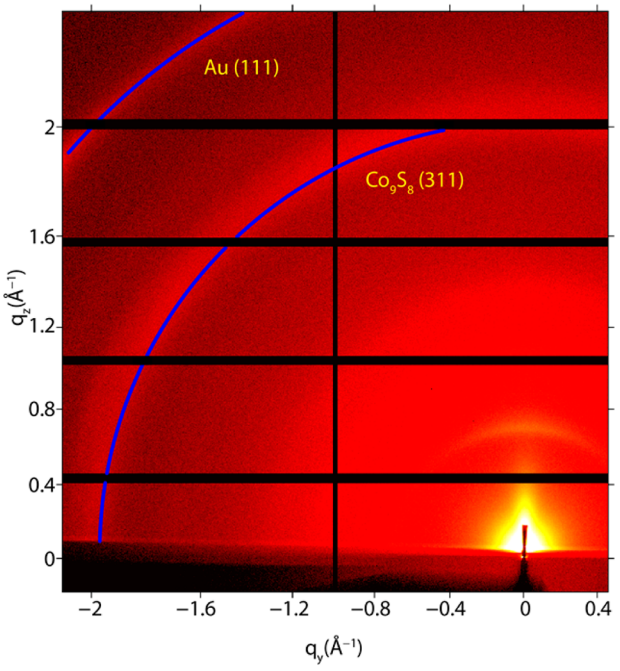

Figure 4. Grazing incidence X-ray diffraction of Co_9S_8 nanofilm prepared from 50 deposition cycles on a Au substrate. Au(111) and Co_9S_8 (311) peaks are indicated with blue lines.

AFM analysis of Co_9S_8 films reveals an RMS roughness of 2.93 nm similar to the 2.90 nm roughness of the polycrystalline gold substrate, indicating a relatively uniform conformal deposit of Co_9S_8 (Figures S13 and S14). Small undulations observed periodically in the AFM image are attributed to buckling of the lattice-mismatched Co_9S_8 layer on the gold substrate,[27] and cross-sectional TEM images of these features are consistent with this assignment (Figure S15). The relatively smooth film morphology observed by AFM is also preserved over large areas of the macroscopic electrode and for thicker films. SEM of a Co_9S_8 film produced by 25 deposition cycles (Figures 5 and S16) reveals a relatively smooth catalyst layer conformally

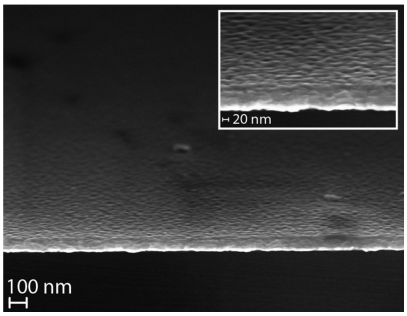

Figure 5. SEM image of a Co_9S_8 nanofilm prepared from 25 deposition cycles on a Au-coated Si substrate recorded at 15° with a zoom-in of the Co_9S_8 surface (inset).

coating the Au substrate. Small undulations observed in the SEM images are reminiscent of those observed in the AFM and cross sectional TEM images on thinner films.

Typically, cobalt sulfide preparations require high temperature colloidal synthesis (>180 °C) or postsynthetic annealing (>300 °C) to produce catalytically active materials.[23] Remarkably, our room-temperature layer-by-layer growth method produces active ORR catalysts without any post-processing of the thin film. Linear sweep voltammograms (LSVs) of a cobalt sulfide film prepared from 10 deposition cycles recorded in O_2-saturated 0.1 M $HClO_4$, (Figure 6a)

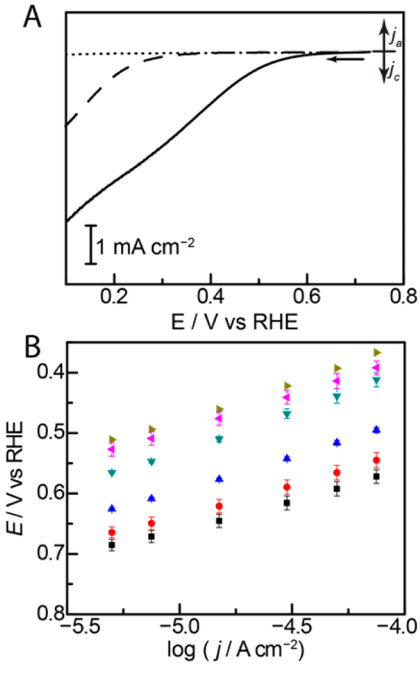

Figure 6. (a) LSVs (5 mV s^{-1} scan rate) of a Au rotating disk electrode decorated with a Co_9S_8 thin film (10 deposition cycles) in O_2 (solid line) and N_2 (dotted line) saturated 0.1 M $HClO_4$ and polycrystalline gold electrode (dotted−dashed line) in O_2-saturated 0.1 M $HClO_4$. (b) Tafel plots of ORR catalysis in O_2-saturated 0.1 M $HClO_4$ electrolyte rotation at 2000 rpm on a Au electrode (brown triangle) and a Au electrode decorated with cobalt sulfide prepared from 1 (pink triangle), 3 (green triangle), 5 (blue triangle), 10 (red circle), and 15 (black square) deposition cycles.

DOI: 10.1021/acscatal.5b00449
ACS Catal. 2015, 5, 3411−3416

display a catalytic wave with onset at 0.6 V. This wave is absent in LSV scans recorded in Ar-saturated electrolyte. Additionally, the ORR catalytic wave onsets at ~0.2 V more positive than the onset of catalysis by the native gold substrate under identical conditions (Figure 6a). Together, these data indicate that the described layer-by-layer growth yields thin films that are catalytically active for the ORR in acidic aqueous electrolyte.

Catalytic activity was probed as a function of film thickness using controlled potential electrolysis at a variety of potentials in the activation-controlled region of the catalytic wave (Figure 6b). Whereas films formed from 1 and 3 deposition cycles show poor performance—low currents at low potentials (high overpotentials)—catalytic activity systematically rises as the film thickness is increased. We observe 1 order of magnitude increase in activity between 1 and 5 deposition cycles and saturation in catalytic activity at ≥10 deposition cycles. Given the smooth surface film morphologies observed by TEM (Figures 3 and S12), SEM (Figures 5 and S16), and AFM (Figures S13 and S14), we do not attribute this change in activity to drastic changes in electroactive surface area. Indeed, across the entire series from 1 to 15 deposition cycles, we observe only a factor of ~1.8 increase in the AFM surface roughness, consistent with preservation of a smooth, conformal surface morphology across a wide range of film thicknesses. Since cobalt sulfide materials are known supercapacitors,[28] conventional double layer capacitance measurements are expected to overestimate the electroactive surface area. Consistent with this expectation, we observe a sudden jump in double layer capacitance from 26 μF cm^{-2} for the bare gold substrate to 84 μF cm^{-2} for a film prepared from three deposition cycles (Figure S17). Between 3 and 10 deposition cycles, the films display similar capacitances, consistent with retention of a smooth surface morphology. Taken together, the data suggest that the rise in catalytic activity of Co_9S_8 between 1 and 10 deposition cycles is due largely to an increase in specific activity rather than an increase in electroactive surface area.

The precise origin of this rise in catalyst specific activity is still under investigation and may be due to several causes. Co_9S_8 displays a high conductivity of 290 S cm^{-1} at room temperature, suggesting that charge transfer resistance through the film plays a negligible role.[29] However, given the complexity of the Co_9S_8 lattice, consisting of a cubic 9.93 Å unit cell containing 68 atoms, the lower specific activity of ultrathin films may be due to incomplete crystallization of Co_9S_8 domains on the electrode surface. Alternatively, increased deposition cycles may be necessary for building up catalytically competent surface facets or defects that exist in low population on ultrathin films. In situ XANES and EXAFS studies are underway to further probe changes in structure as a function of film thickness. Notwithstanding, the nominal plateau in catalytic activity at ≥10 deposition cycles is consistent with ORR catalysis confined to the Co_9S_8|electrolyte interface and suggests that 10 deposition cycles of this material is sufficient to maximize specific activity.

Unlike catalyst-impregnated carbon composites, which are subject to inhomogeneous diffusion limitations,[24] the smooth morphology of our Co_9S_8 thin films ensures uniform transport of reactants to the surface, permitting the collection of electrokinetic data over a wide range of current densities, a prerequisite of mechanistic studies of electrocatalysis. Exploiting this key advantage of E-ALD thin films, we constructed a Tafel plot of overpotential, η, versus the log of the activation-controlled current density, j, for ORR on an optimal Co_9S_8 film prepared from 10 deposition cycles (Figure 7). To ensure that all measurements of catalytic rate represented a true steady

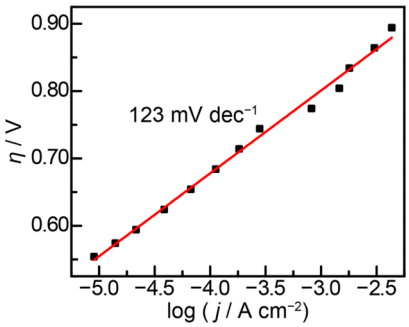

Figure 7. Tafel plot of a Co_9S_8 thin film prepared from 10 deposition cycles conducted in O_2-saturated, 0.1 M $HClO_4$ while rotating at 2000 rpm. For η > 0.75 V, activation-controlled current densities were obtained by extrapolating Koutecky–Levich plots to infinite rotation rate.

state, we conducted controlled potential electrolyses across a series of potentials spanning the catalytic wave in Figure 6a. In all cases, the catalytic current reached a steady state within 30 s throughout the potential range explored. At higher overpotentials, η > 0.75 V, the reaction proceeds under mixed activation and transport control and thus, we extrapolated Koutecky–Levich plots of reciprocal current density, j^{-1}, vs the reciprocal square root of rotation rate, $\omega^{-1/2}$, to the y-axis, representing infinite rotation rate,[30] to extract the activation controlled current density (representative Koutecky–Levich plots are shown in Figure S18). Despite the low catalyst loading (<1 μg cm^{-2}), film-decorated electrodes exhibit remarkable robustness over the ~60 min time scale of Tafel data collection even in caustic 0.1 M $HClO_4$. Indeed, controlled potential electrolysis at the highest overpotential sampled in the Tafel plot reveals sustained catalytic activity over the course of an hour (Figure S19). Together these observations indicate that these films are well-suited to detailed mechanistic investigations of ORR kinetics.

In line with the well-defined morphology of our films, we observe linear Tafel data over a ~0.35 V range in potential and 2.5 decade range in current density (Figure 7). We calculate a Tafel slope of ~123 mV decade^{-1}, consistent with ORR catalysis proceeding via a rate-limiting one-electron transfer to O_2.[31] While more detailed studies are under way to extract a complete mechanistic model, these data, taken together with the surface roughness of the gold substrate (see the SI), allow us to estimate an ORR-specific activity of 20.4 μA cm^{-2} at 600 mV vs RHE for polycrystalline Co_9S_8. Given that LTMCs are supercapacitors[28] and lack well-defined adsorption probes of electrochemically active surface area, this specific activity estimate is, to our knowledge, unprecedented for ORR catalysis on this class of materials and serves as a benchmark for systematic improvements in catalytic performance.

Practical ORR catalysts must be highly active and immune to poisoning agents such as methanol that may crossover from the anode compartment of the fuel cell.[32] Co_9S_8 nanofilms demonstrate remarkable poison resistance, showing no change in ORR activity even in the presence of 0.1 M methanol (Figure S20).

Since our cobalt sulfide thin films are morphologically well-defined, rotating ring disk electrode (RRDE) experiments can

DOI: 10.1021/acscatal.5b00449
ACS Catal. 2015, 5, 3411−3416

be used to provide an accurate estimate of intrinsic catalytic selectivity for four-electron versus two-electron reduction of O_2.[33] Such measurements are ambiguous for mesostructured carbon-supported nanoparticles due to convolution from secondary reduction or disproportionation of peroxide intermediates before they escape the carbon host.[9] In contrast, studies on planar electrodes yield unambiguous results. Figure 8

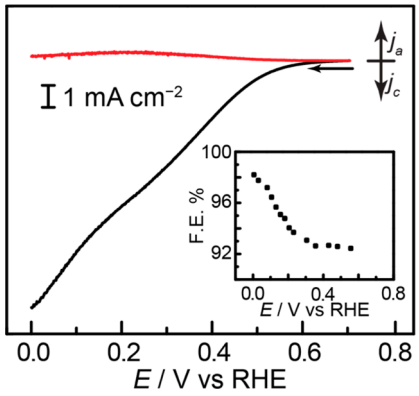

Figure 8. LSVs (5 mV s^{-1} scan rate) of a rotating ring disk electrode. Disk current for ORR catalysis from a cobalt sulfide thin film generated from 10 deposition cycles (black), Pt ring current for H_2O_2 oxidation to O_2 (red), and percent faradaic efficiency for H_2O production (inset).

shows a linear sweep voltammogram of cobalt sulfide-catalyzed ORR overlaid with the anodic current observed on a platinum ring electrode polarized at 1.0 V such that peroxide produced at the rotating disk is rapidly back-oxidized to O_2 at the ring. Based on the independently determined collection efficiency of the RRDE, we determined that these cobalt sulfide thin films display high selectivity, between 90 and 100%, for four electron reduction of O_2 to H_2O throughout the potential range explored (Figure 8, inset). These data provide, for the first time, clear evidence that Co_9S_8 is able to mediate direct four-electron reduction of O_2 to H_2O with high selectivity under acidic conditions.[32]

CONCLUSIONS

We report a facile, E-ALD method for preparing crystalline Co_9S_8 nanofilms at room temperature. As prepared, the films are active for the oxygen reduction reaction and their smooth conformal morphology enables, for the first time, accurate measurement of the ORR specific activity of Co_9S_8. Electrokinetic studies establish that oxygen reduction catalysis by Co_9S_8 proceeds via rate-limiting one-electron transfer to O_2 with high selectivity for four-electron reduction to water and high tolerance to methanol. The uniform and tunable catalyst morphology afforded by this synthetic route opens the door to detailed mechanistic investigations of metal chalcogenide electrocatalysts, and the layer-by-layer method of synthesis permits rapid and precise tuning of catalyst composition, allowing for systematic optimization of catalytic activity and selectivity.

ASSOCIATED CONTENT

Supporting Information

The Supporting Information is available free of charge on the ACS Publications website at DOI: 10.1021/acscatal.5b00449.

Full synthetic protocols, additional electrochemical characterization, and additional microscopy characterization of the thin films (PDF)

AUTHOR INFORMATION

Corresponding Author

*E-mail: yogi@mit.edu.

Notes

The authors declare no competing financial interest.

ACKNOWLEDGMENTS

This research was supported by the Aramco Services Company through an MIT Energy Initiative Grant, the NSF under award CHE-1454060, and by the MIT Department of Chemistry through junior faculty funds for Y.S. This work made use of the MRSEC Shared Experimental Facilities at MIT and the Center for Nanoscale Systems at Harvard, which are supported in part by the NSF under awards DMR-0819762 and ECS-0335765, respectively. We gratefully acknowledge Shoji Hall, Carter Abney, Sophie Liu, and Nicolas Antoniou for assistance with SEM analysis, ICP-MS analysis, gold electrode fabrication, and TEM sample preparation, respectively.

REFERENCES

(1) Gewirth, A. A.; Thorum, M. S. *Inorg. Chem.* **2010**, *49*, 3557−3566.
(2) Nørskov, J. K.; Rossmeisl, J.; Logadottir, A.; Lindqvist, L.; Kitchin, J. R.; Bligaard, T.; Jónsson, H. *J. Phys. Chem. B* **2004**, *108*, 17886−17892.
(3) Conway, B. E.; Tilak, B. V. *Electrochim. Acta* **2002**, *47*, 3571−3594.
(4) Nørskov, J. K.; Bligaard, T.; Logadottir, a.; Kitchin, J. R.; Chen, J. G.; Pandelov, S.; Stimming, U. *J. Electrochem. Soc.* **2005**, *152*, J23.
(5) Bockris, J. O.; Otagawa, T. *J. Phys. Chem.* **1983**, *87*, 2960−2971.
(6) Surendranath, Y.; Nocera, D. G. Oxygen Evolution Reaction Chemistry of Oxide-Based Electrodes. *Progress in Inorganic Chemistry*; Wiley, 2011; Vol. 57, pp 505−560; DOI: 10.1002/9781118148235.ch9.
(7) (a) Soderberg, J. N.; Co, A. C.; Sirk, A. H. C.; Birss, V. *J. Phys. Chem. B* **2006**, *110*, 10401−10410. (b) Banham, D.; Feng, F.; Fürstenhaupt, T.; Pei, K.; Ye, S.; Birss, V. *J. Power Sources* **2011**, *196*, 5438−5445. (c) Banham, D.; Feng, F.; Pei, K.; Ye, S.; Birss, V. *J. Mater. Chem. A* **2013**, *1*, 2812−2820.
(8) (a) Yu, Z.; Du, J.; Guo, S.; Zhang, J.; Matsumoto, Y. *Thin Solid Films* **2002**, *415*, 173−176. (b) Wang, J.; Ng, S. H.; Wang, G. X.; Chen, J.; Zhao, L.; Chen, Y.; Liu, H. K. *J. Power Sources* **2006**, *159*, 287−290.
(9) (a) Neumann, C. C. M.; Laborda, E.; Tschulik, K.; Ward, K. R.; Compton, R. G. *Nano Res.* **2013**, *6*, 511−524. (b) Bonakdarpour, A.; Lefevre, M.; Yang, R.; Jaouen, F.; Dahn, T.; Dodelet, J.-P.; Dahn, J. R. *Electrochem. Solid-State Lett.* **2008**, *11*, B105−B108.
(10) Herrero, E.; Buller, L. J.; Abruña, H. D. *Chem. Rev.* **2001**, *101*, 1897−1930.
(11) Schmidt, T. J.; Gasteiger, H. A.; Stab, G. D.; Urban, P. M.; KoIb, D. M.; Behm, R. J. *J. Electrochem. Soc.* **1998**, *145*, 2354−2358.
(12) Kern, W., Vossen, J. L., Eds. *Thin Film Processes II*; Academic Press: Boston, MA, 1991.
(13) Nogues, C.; Wanunu, M. *Surf. Sci.* **2004**, *573*, L383−L389.
(14) Rodriguez, P.; Kwon, Y.; Koper, M. T. M. *Nat. Chem.* **2012**, *4*, 177−182.
(15) Liu, Y.; Cheng, H.; Lyu, M.; Fan, S.; Liu, Q.; Zhang, W.; Zhi, Y.; Wang, C.; Xiao, C.; Wei, S.; Ye, B.; Xie, Y. *J. Am. Chem. Soc.* **2014**, *136*, 15670−15675.
(16) Gao, M.-R.; Jiang, J.; Yu, S.-H. *Small* **2012**, *8*, 13−27.
(17) Kibsgaard, J.; Chen, Z.; Reinecke, B. N.; Jaramillo, T. F. *Nat. Mater.* **2012**, *11*, 963−969.

DOI: 10.1021/acscatal.5b00449
ACS Catal. 2015, 5, 3411−3416

(18) Merki, D.; Vrubel, H.; Rovelli, L.; Fierro, S.; Hu, X. *Chem. Sci.* **2012**, *3*, 2515−2525.
(19) Sun, Y.; Liu, C.; Grauer, D. C.; Yano, J.; Long, J. R.; Yang, P.; Chang, C. J. *J. Am. Chem. Soc.* **2013**, *135*, 17699−17702.
(20) Chan, K.; Tsai, C.; Hansen, H. a.; Nørskov, J. K. *ChemCatChem* **2014**, *6*, 1899−1905.
(21) Asadi, M.; Kumar, B.; Behranginia, A.; Rosen, B. a; Baskin, A.; Repnin, N.; Pisasale, D.; Phillips, P.; Zhu, W.; Haasch, R.; Klie, R. F.; Král, P.; Abiade, J.; Salehi-Khojin, A. *Nat. Commun.* **2014**, *5*, 4470.
(22) (a) Gregory, B. W.; Stickney, J. L. *J. Electroanal. Chem. Interfacial Electrochem.* **1991**, *300*, 543−561. (b) Colletti, L. P.; Tekley, D.; Stickney, J. L. *J. Electroanal. Chem.* **1994**, *369*, 145−152.
(23) Wagner, F. T.; Lakshmanan, B.; Mathias, M. F. *J. Phys. Chem. Lett.* **2010**, *1*, 2204−2219.
(24) Behret, H.; Binder, H.; Sandstede, G. *Electrochim. Acta* **1975**, *20*, 111−117.
(25) Sidik, R. A.; Anderson, A. B. *J. Phys. Chem. B* **2006**, *110*, 936−941.
(26) (a) Feng, Y.; He, T.; Alonso-Vante, N. *Chem. Mater.* **2008**, *20*, 26−28. (b) Feng, Y.; He, T.; Alonso-Vante, N. *ECS Trans* **2008**, *11*, 67−73. (c) Wang, H.; Liang, Y.; Li, Y.; Dai, H. *Angew. Chem., Int. Ed.* **2011**, *50*, 10969−10972. (d) Jirkovský, J.; Björling, A.; Ahlberg, E. *J. Phys. Chem. C* **2012**, *116*, 24436−24444. (e) Liu, Q.; Zhang, J. *CrystEngComm* **2013**, *15*, 5087−5092. (f) Zhao, C.; Li, D.; Feng, Y. *J. Mater. Chem. A* **2013**, *1*, 5741−5746. (g) Mahmood, N.; Zhang, C.; Jiang, J.; Liu, F.; Hou, Y. *Chem. - Eur. J.* **2013**, *19*, 5183−5190.
(27) (a) Loglio, F.; Innocenti, M.; Jarek, A.; Caporali, S.; Pasquini, I.; Foresti, M. L. *J. Electroanal. Chem.* **2010**, *638*, 15−20. (b) Biçer, M.; Şişman, I. *Appl. Surf. Sci.* **2011**, *257*, 2944−2949. (c) Henríquez, R.; Gómez, H.; Riveros, G.; Guillemoles, J. F.; Froment, M.; Lincot, D. *J. Phys. Chem. B* **2004**, *108*, 13191−13199.
(28) (a) Yuan, C.; Shen, L.; Zhang, F.; Lu, X.; Li, D.; Zhang, X. *J. Colloid Interface Sci.* **2010**, *349*, 181−185. (b) Justin, P.; Ranga Rao, G. *Int. J. Hydrogen Energy* **2010**, *35*, 9709−9715. (c) Bao, S.-J.; Li, C. M.; Guo, C.-X.; Qiao, Y. *J. Power Sources* **2008**, *180*, 676−681. (d) Yang, Z.; Chen, C.-Y.; Chang, H.-T. *J. Power Sources* **2011**, *196*, 7874−7877. (e) Tao, F.; Zhao, Y.-Q.; Zhang, G.-Q.; Li, H.-L. *Electrochem. Commun.* **2007**, *9*, 1282−1287. (f) Wang, Q.; Jiao, L.; Du, H.; Yang, J.; Huan, Q.; Peng, W.; Si, Y.; Wang, Y.; Yuan, H. *CrystEngComm* **2011**, *13*, 6960. (g) Yuan, C.; Gao, B.; Su, L.; Chen, L.; Zhang, X. *J. Electrochem. Soc.* **2009**, *156*, A199.
(29) Kumar, N.; Raman, N.; Sundaresan, A. *Z. Anorg. Allg. Chem.* **2014**, *640*, 1069−1074.
(30) Bard, A. J.; Faulkner, L. R. *Electrochemical Methods Fundamentals and Applications*, 2nd ed.; John Wiley & Sons: New York, 2001; pp 340−344.
(31) Gileadi, E. *Physical Electrochemistry*; Wiley-VCH: Weinheim, 2011; pp 1−92.
(32) Ahmed, M.; Dincer, I. *Int. J. Energy Res.* **2011**, *35*, 1213−1228.
(33) Albery, W. J.; Hitchman, M. L. *Ring-Disk Electrodes*; Oxford University Press: London, 1971; pp 71−90.

DOI: 10.1021/acscatal.5b00449
ACS Catal. 2015, 5, 3411−3416